# Current-phase relation and phase-dependent conductance of superconducting point contacts from rf impedance measurements*

Robert Rifkin and Bascom S. Deaver, Jr.
*Department of Physics, University of Virginia, Charlottesville, Virginia 22901*
(Received 24 November 1975)

The rf impedance of superconducting point contacts has been measured as a function of the quantum-mechancial phase difference $\phi$ across the point contact. By representing the point contact as a parallel combination of an inductor $\mathcal{L}(\phi) = (\hbar/2e)(\partial I_p/\partial\phi)^{-1}$ and a resistor $R \equiv 1/G(\phi)$ the current-phase relation $I_p(\phi)$ and the phase-dependent conductance $G(\phi)$ have been determined from measurements at 30 MHz on phase-biased niobium point contacts. For point contacts with sufficiently small critical current $I_c$, the inductance was $\mathcal{L}(\phi) = \hbar/2eI_c\cos\phi$ yielding the expected negative inductance branch for $\pi/2 \leq \phi \leq \pi$ and a sinusoidal current-phase relation. For larger critical currents there were departures from the sinusoidal form for the measured $I_p(\phi)$. There was a phase-dependent conductance that is an increasing function of $\phi$ corresponding to a negative coefficient for the $\cos\phi$ term in the Josephson current.

## I. INTRODUCTION

The Josephson equations describing the total current $I$ flowing between two weakly connected superconductors can be written in the form

$$I = I_c \sin\phi + G_0(1 + \alpha\cos\phi)V\,, \tag{1}$$

$$\frac{\partial\phi}{\partial t} = \frac{2e}{\hbar}V\,, \tag{2}$$

where $\phi$ is the gauge-invariant phase difference between the wave functions of the two superconductors, $I_c$ is the critical current, $G_0$ is the normal conductance of the weak link, and $\alpha$ is the ratio of conductance associated with the phase-dependent term to the normal conductance ($\sigma_1/\sigma_0$ in Josephson's notation).[1] In general the coefficients $I_c$, $G_0$, and $\alpha$ depend on voltage and temperature, however, we will assume that for small voltages relative to the energy gap and fixed temperature they are constants; we also assume a uniform current density.

The total current $I$ can be considered to be the sum of two contributions, a pair current $I_p(\phi) = I_c\sin\phi$ and a quasiparticle current $I_q(\phi) = G(\phi)V$ determined by a phase-dependent conductance $G(\phi)$. Many experiments have demonstrated implicitly good qualitative agreement with a sinusoidal current-phase relation $I_p(\phi)$. Some relatively direct measurements[2,3] of $I_p(\phi)$ have shown nearly sinusoidal form for several types of weak links, and extremely good agreement with the sinusoidal relation has been found for oxidized Nb point contacts.[4]

For the phase-dependent quasiparticle current the situation is not so clear. Recent experiments[5-8] have demonstrated qualitatively the existence of the $\cos\phi$ term with a coefficient $\alpha \simeq -1$. However, the results are still open to some question. For example, none of the experiments provide strong concurrent evidence that the various weak links used do indeed have sinusoidal current-phase relations. Thus it is not known what form to expect for the corresponding $G(\phi)$. Moreover, some confusion still exists about relating the microscopic theory to the experiments.[9,10]

In this paper we discuss a technique for obtaining both $I_p(\phi)$ and $G(\phi)$ from measurements of the impedance of a weak link and we report results of measurements on phase-biased Nb point contacts made at 30 MHz.

## II. CIRCUIT MODEL

If a steady current $I_0 < I_c$ is passed through a weak link the phase difference across the weak link will be fixed at a particular value $\phi_0$. If in addition a very small alternating current $I_{ac} \ll I_c$ is passed through the weak link, an ac voltage $V_{ac}$ will be developed across it, and the voltage is related to the alternating current by

$$V_{ac} = I_{ac}\,Z(\phi_0)\,.$$

In this small-signal limit the junction can be regarded as an impedance $Z(\phi_0)$ whose value is determined by the fixed value of the phase difference $\phi_0$.

By use of a current bias the phase difference $\phi_0$ can be fixed stably only at values between zero and $\frac{1}{2}\pi$. However, if the weak link is incorporated into a superconducting ring (Fig. 1) with sufficiently small inductance $L$, the phase can be fixed stably at any value by fixing the value of an externally applied flux $\Phi_x$. The relation between $\phi$ and $\Phi_x$ is established through the requirement of fluxoid

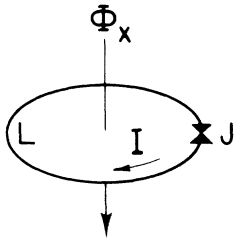


FIG. 1. Diagram of weak link $J$ in superconducting ring of inductance $L$ carrying a current $I$. An externally applied flux $\Phi_x$ passes through the ring.

quantization which can be written

$$(\Phi_0/2\pi)\phi + LI(\phi) + \Phi_x = n\Phi_0, \tag{3}$$

where $\Phi_0 \equiv h/2e$ is the flux quantum and $n$ is an integer. For $I_p(\phi) = I_c \sin\phi$, solving Eq. (3) for $\phi$ gives the well-known result that $\phi$ is a continuous function of $\Phi_x$ if $LI_c < \Phi_0/2\pi$. Thus the junction can be phase biased by fixing the value of $\Phi_x$.

In the experiments to be described below both a steady flux and an extremely small alternating flux are applied so

$$\phi \simeq \phi_0 + \phi_1 \cos\omega t. \tag{4}$$

The corresponding current and the voltage across the junction can be obtained by inserting the phase, Eq. (4), into Eqs. (1) and (2). For very small $\phi_1$, keeping only the first-order terms yields the result that there are three components of the current: (i) a dc part $I_c \sin\phi_0$, (ii) a component at frequency $\omega$ for which the current and voltage are 90° out of phase. This is the pair current which is purely reactive and for which

$$V_{ac}/I_p = \omega\Phi_0/2\pi I_c \cos\phi_0. \tag{5}$$

The pair current corresponds to the current flow through a phase-dependent inductor $\mathfrak{L}(\phi)$. This well-known result can be obtained more simply by combining $I_p(\phi)$ with Eq. (2) to find $V = \mathfrak{L}(\phi)\,\partial I_p(\phi)/\partial t$ where

$$\mathfrak{L}(\phi) = \frac{\hbar}{2e}\left(\frac{\partial I_p(\phi)}{\partial\phi}\right)^{-1}. \tag{6}$$

A measurement of $\mathfrak{L}(\phi)$ is in essence a determination of the current-phase relation $I_p(\phi)$. The first qualitative measurements of this parametric inductance were reported by Silver and Zimmerman.[11] (iii) a component at frequency $\omega$ for which the current and voltage are in phase. This is the quasiparticle current for which

$$V_{ac}/I_q = 1/G_0(1 + \alpha\cos\phi_0). \tag{7}$$

It is possible then to represent the weak link as an impedance $Z(\phi)$ consisting of a parallel combination of $\mathfrak{L}(\phi)$ and $R(\phi)$ where

$$\mathfrak{L}(\phi) = \Phi_0/2\pi I_c \cos\phi \tag{8}$$

and

$$R(\phi) \equiv 1/G(\phi) = 1/G_0(1 + \alpha\cos\phi). \tag{9}$$

The conditions for this impedance representation to be valid are $\phi_1 \ll 2\pi$, or equivalently $2e|V_{ac}|/\hbar\omega \ll 1$, or $|I_{ac}| \ll I_c$.

In our experiments the superconducting ring containing a weak link was coupled to a high-$Q$ tank circuit through mutual inductance $M$ as shown in Fig. 2(a). We have not included any capacitance in the model because reasonable estimates indicate its effect to be negligible for our experiments. By reflecting the ring impedance into the tank circuit, we can represent the effect of the ring on the tank

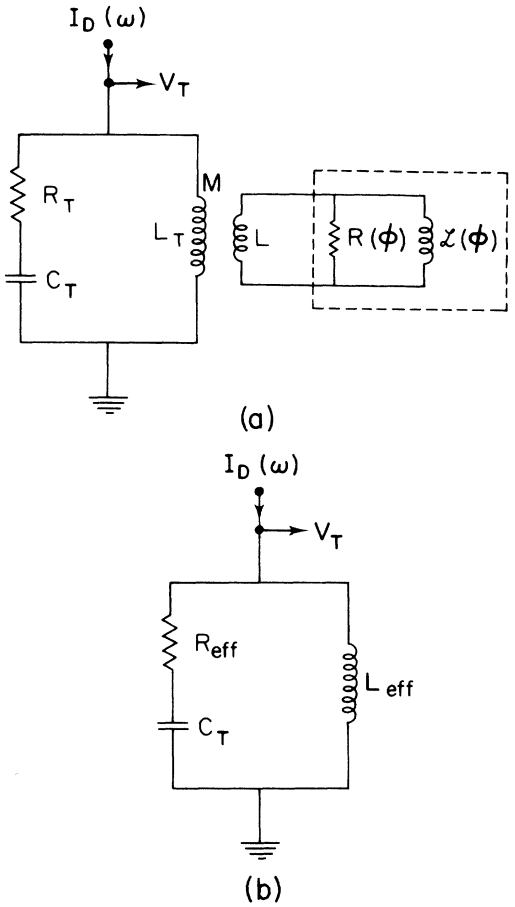


FIG. 2. (a) Model of weak link in superconducting ring coupled to tank circuit through mutual inductance $M$. The two paralleled impedances within the dashed box represent the weak link. (b) Schematic diagram of tank circuit showing effective impedances used to represent the effect of coupling the superconducting ring with weak link to tank circuit.

in terms of the effective impedances shown in Fig. 2(b), where $L_{\text{eff}}$ and $R_{\text{eff}}$ are found by standard circuit theory to be

$$L_{\text{eff}} = L_T - \frac{R^2M^2(\mathfrak{L}+L) + \omega^2M^2\mathfrak{L}^2L}{R^2(\mathfrak{L}+L)^2 + \omega^2\mathfrak{L}^2L^2} \tag{10}$$

and

$$R_{\text{eff}} = R_T + \frac{R\omega^2M^2\mathfrak{L}^2}{R^2(\mathfrak{L}+L)^2 + \omega^2\mathfrak{L}^2L^2}\,. \tag{11}$$

The effective impedances $R_{\text{eff}}$ and $L_{\text{eff}}$ are the quantities actually measured in the experiments by measuring the voltage $V_T$ across the tank when it is driven with an rf current $I_D(\omega)$ (Fig. 2). By inverting Eqs. (10) and (11) we obtain $\mathfrak{L}$ and $R$ in terms of $L_{\text{eff}}$ and $R_{\text{eff}}$:

$$\mathfrak{L} = \frac{(R_{\text{eff}}-R_T)^2L^2 + \omega^2[M^2 + (L_{\text{eff}}-L_T)L]^2}{-\omega^2(L_{\text{eff}}-I_T)[M^2 + (L_{\text{eff}}-L_T)L] - (R_{\text{eff}}-R_T)^2L}\,, \tag{12}$$

$$R = \frac{(R_{\text{eff}}-R_T)^2L^2 + \omega^2[M^2 + (L_{\text{eff}}-L_T)L]^2}{(R_{\text{eff}}-R_T)M^2}\,. \tag{13}$$

## III. EXPERIMENTS

As shown in Fig. 3 the weak link used for the experiments was a Nb point contact incorporated into a ring of toroidal configuration. This configuration was used both because it makes possible an extremely low inductance $L$ for the superconducting ring and because this geometry minimized coupling to extraneous fields. The screw tip was very blunt to reduce the total inductance. There were two toroidal cavities in a niobium block, one with mean diameter $D_1 = 18$ mm and cross-sectional diameter $d = 1.0$ mm and the second of diameter $D_2 = 16$ mm and cross-sectional area of ~ 0.2 mm$^2$. Both cavities contained coils wound with 51-$\mu$-diam niobium wire. The smaller coil was used as the inductor $L_T$ of the tank circuit. The total inductance of the toroidal ring with the point contact shorted was measured to be $1.0\times10^{-10}$ H. This low inductance permitted analysis of point contacts with critical currents as high as ~ 3 $\mu$A while still remaining in the regime $LI_c < \Phi_0/2\pi$.

The rf drive coil ($L_T$ in Fig. 2) had a calculated inductance of $1.6\times10^{-7}$ H which when combined with a 100-pF capacitor and ~ 80 pF of distributed

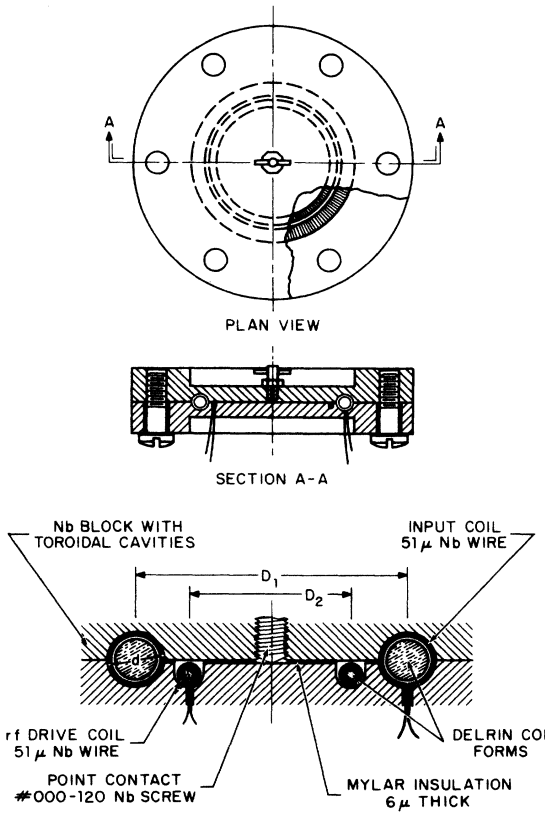


FIG. 3 Detailed drawing of the superconducting ring showing Nb block with concentric toroidal cavities and Nb point contact.

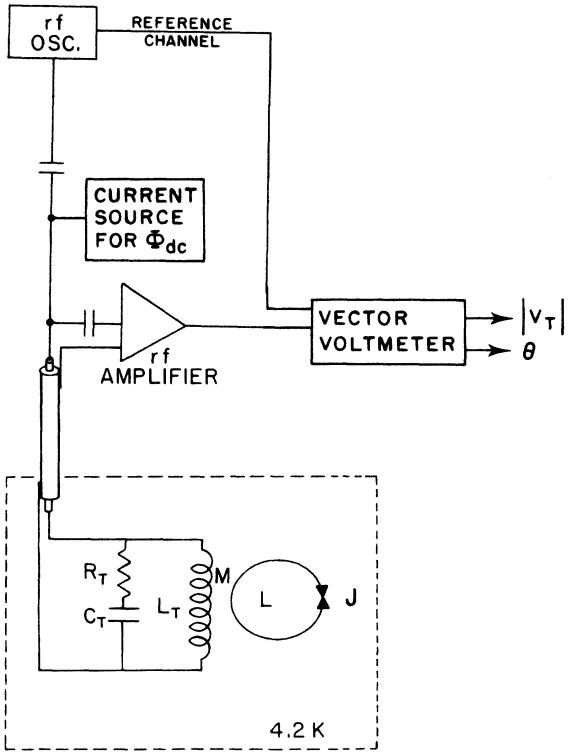


FIG. 4. Block diagram of experimental set up showing technique employed to extract magnitude and phase of rf voltage across the tank circuit.

capacitance formed a tank circuit resonant at ~ 30 MHz. With $Q \simeq 150$ the tank circuit served to improve the match of the low impedance of the ring to that of the rf amplifier.

As shown in Fig. 4, an rf oscillator coupled to the tank through an extremely small capacitor provided a constant current source. To set the phase $\phi$ a steady external flux $\Phi_{dc}$ was applied to the toroidal ring by a dc current in either the input coil or the rf drive coil (Fig. 3). The components shown within the dashed box in Fig. 4 were contained in a copper chamber filled with helium gas. This chamber, which was immersed in liquid helium, was completely surrounded by lead foil to serve as a superconducting shield. The helium Dewar was located inside a pair of concentric mu-metal magnetic shields and all electrical leads except the rf coax passed through rf filters as they entered the cryostat.

The circuit of Fig. 2(a) is the standard one for an rf superconducting quantum interference device (SQUID). In contrast to operation as a SQUID however, for our experiments the rf drive current $I_D$ was kept as small as possible so that the ac current in the superconducting ring was much less than the critical current of the weak link. The variation of $V_T$ with $\Phi_{dc}$ was then a measure of $Z(\phi)$.

When operating the SQUID as a magnetometer it is most common to set $I_D$ to a value $(I_D)_{max}$ which maximizes the sensitivity of $V_T$ to variations of $\Phi_{dc}$. This condition corresponds approximately to an rf current in the superconducting ring with amplitude $I_c$ and is obtained when the Bessel function determining the dependence of $V_T$ on $I_D$ is at its first maximum. A convenient check on the assumption that we were operating in the small signal limit was obtained by determining $(I_D)_{max}$ and then insuring that $I_D << (I_D)_{max}$. All the measurements reported here were made with $I_D \simeq \frac{1}{40}(I_D)_{max}$. Another operational check on the small-signal assumption was that for sufficiently small drive current the values determined for $Z(\phi)$ were independent of $I_D$.

The quantities $L_{eff}$ and $R_{eff}$ that served as the input data to Eqs. (12) and (13) for determining $R(\phi)$ and $\mathcal{L}(\phi)$ were determined in two ways. For the first the detected output from the rf amplifier (Fig. 4) was plotted as a function of the frequency of the drive current giving a resonant response curve. From the resonant frequency $\nu_0$ and the $Q$ determined from this curve $L_{eff}$ and $R_{eff}$ were obtained. A family of such curves for various values of $\Phi_{dc}$ are shown in Fig. 5. Data of this type were used by Vincent and Deaver[7] for the first determination of the phase-dependent conductance of point contacts.

For most of our experiments data of this type was displayed on an oscilloscope and served as a quick qualitative method for determining $I_c$ and $G_0$. It was found that $I_c$ was roughly proportional to $\Delta\nu_0$, the shift of the resonant frequency between $\Phi_{dc} = n\Phi_0$ and $\Phi_{dc} = (n + 1/2)\Phi_0$, where $n$ is an integer. [$Z(\phi)$ is periodic with one period corresponding to a variation of $\Phi_{dc}$ by one flux quantum $\Phi_0$.] Correspondingly, $G_0$ was roughly proportional to $\Delta Q$ for the same change in $\Phi_{dc}$. With resonant frequencies near 30 MHz we observed values of $\Delta\nu_0/\nu_0$ from less than $10^{-3}$ up to $10^{-2}$ representing critical currents from less than 1 to 5 $\mu$A, respectively. Point contacts with $I_c < 1.5\ \mu$A showed no measurable $\Delta Q$ implying $G_0 < 2\ \Omega^{-1}$. Point contacts with large $I_c$ showed $Q$ variations as large as a factor of four implying $G_0 \simeq 5\ \Omega^{-1}$.

A second more precise technique was used for all quantitative determinations of $L_{eff}$ and $R_{eff}$. As shown in Fig. 4 an rf vector voltmeter (HP Model 8405A) was used to measure the magnitude $|V_T|$ and phase angle $\theta$ of the tank voltage relative to drive current. The instrument provided $|V_T|$ and $\theta$ directly and in addition gave two 20-kHz outputs with the same amplitude and phase relations as the input rf signals. Improved signal to noise ratio was obtained by using a lock-in amplifier to measure the magnitude and phase of these outputs with longer integration time than that of the voltmeter itself.

Numerical values for the parameters in Eqs.

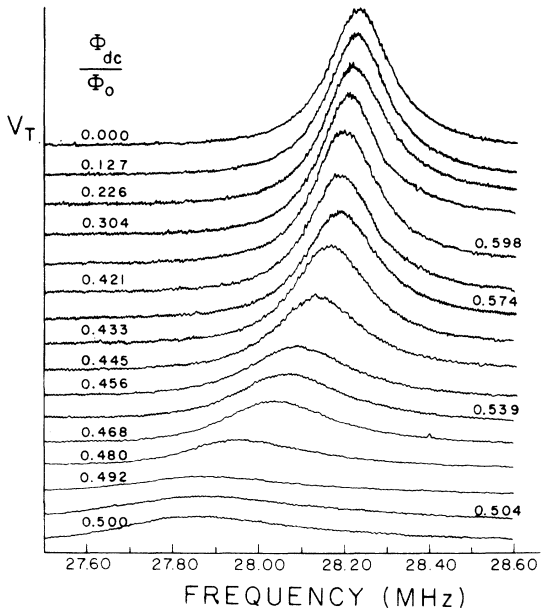


FIG. 5. Plot of $V_T$ vs frequency at various $\Phi_{dc}$ taken in the low signal limit. The origin has been shifted vertically for the different values of $\Phi_{dc}/\Phi_0$.

(12) and (13) were obtained as follows: The tank inductance $L_T$ was calculated from standard formulas. Measurements of the resonant frequency and $Q$ with the point contact open were used to obtain $C_T$ and $R_T$. The mutual inductance $M$ was determined by measuring the dc current $I_1$ in the tank coil required to give one period of the periodic variation of $V_T(\Phi_{dc})$ which has period $\Phi_0$. Then $I_1 = M\Phi_0$. We found $M = 3.65 \times 10^{-10}$ H.

The inductance $L$ of the toroidal ring was determined by measuring the change in tank impedance as the point contact was changed from open to shorted. Both the resonant-response-curve technique and the vector voltmeter measurements were used to determine this impedance change, giving values of $L$ within 5% of each other and yielding $L = (1.0 \pm 0.1) \times 10^{-10}$ H.

The experimental data and Eqs. (12) and (13) permit the direct determination of $\mathcal{L}$ and $R$ as functions of the external flux $\Phi_{dc}$. To obtain $\mathcal{L}(\phi)$ and $R(\phi)$ requires a knowledge of $\phi(\Phi_{dc})$ which is established by the condition of fluxoid quantization Eq. (3) together with the data $\mathcal{L}(\Phi_{dc})$. The relationship $\phi(\Phi_{dc})$ can be obtained by differentiating Eq. (3) with respect to $\Phi_{dc}$ (in the small signal limit $\Phi_x \simeq \Phi_{dc}$) using the definition of $\mathcal{L}(\phi)$, Eq. (6), and integrating to find

$$\phi(\Phi_{dc}) = \int_0^{\Phi_{dc}} [\,1 + L/\mathcal{L}(\Phi'_{dc})\,]^{-1} d\Phi'_{dc} \,. \qquad (14)$$

Numerically integrating the data thus yields the needed relationship $\phi(\Phi_{dc})$ which in turn can be used to express the data $\mathcal{L}(\Phi_{dc})$ as the desired function $\mathcal{L}(\phi)$ and also by substituting into Eq. (3) to obtain the current-phase relation $I_p(\phi)$ for the weak link. Correspondingly the data $G(\Phi_{dc})$ can be expressed as $G(\phi)$.

This discussion has ignored the effects of thermal fluctuations and noise. The quantity actually measured is a time average of $\mathcal{L}(\phi)$ over some distribution of fluctuations in $\phi$, and the current-phase relation deduced from the measurements are correspondingly affected. Jackel *et al.*[4] have analyzed in detail the effects of fluctuations on the current-phase relation determined from measurements of the total flux through a superconducting ring as a function of the externally applied flux. In contrast to their experiment which in essence measures the time average of $I_p(\phi)$, our experiments measure the time average of $\mathcal{L}(\phi)$ which is a derivative of $I_p(\phi)$. We have simulated the effects of fluctuations on a computer with an assumed sinusoidal current-phase relation and find that for sufficiently small critical currents the effects are probably too small to be observed within our precision, however for larger critical currents, particularly when $\phi(\Phi_{dc})$ is multivalued, the effects are very pronounced and consistent with the conclusions of Jackel *et al.*

With the toroidal device diagrammed in Fig. 3 we have used several different Nb screws for semiquantitative measurements of the impedance of well over a hundred settings of the point contact with critical currents in the range 1–5 $\mu$A. We have obtained detailed data, $\mathcal{L}(\Phi_{dc})$ and $G(\Phi_{dc})$ for twenty different settings. It is convenient to discuss the results in terms of two general groupings: (i) Point contacts with critical current of about 1 $\mu$A, which gave good agreement with a sinusoidal current-phase relation. For these data the parameter $\epsilon = 2\pi L I_c/\Phi_0$ was approximately 0.3 and $\phi(\Phi_{dc})$ was a continuous function. Unfortunately, for these cases we did not have sufficiently good signal to noise ratio to permit a determination of $G$. (ii) Point contacts with critical currents in the range 3–5 $\mu$A for which the measurements of $\mathcal{L}(\phi)$ lead to an apparently nonsinusoidal current-phase relation. For these cases a phase-dependent conductance $G(\phi)$ was observed.

Figure 6(a) shows $\mathcal{L}(\Phi_{dc})$ data for a point contact representative of the first group. The inductance

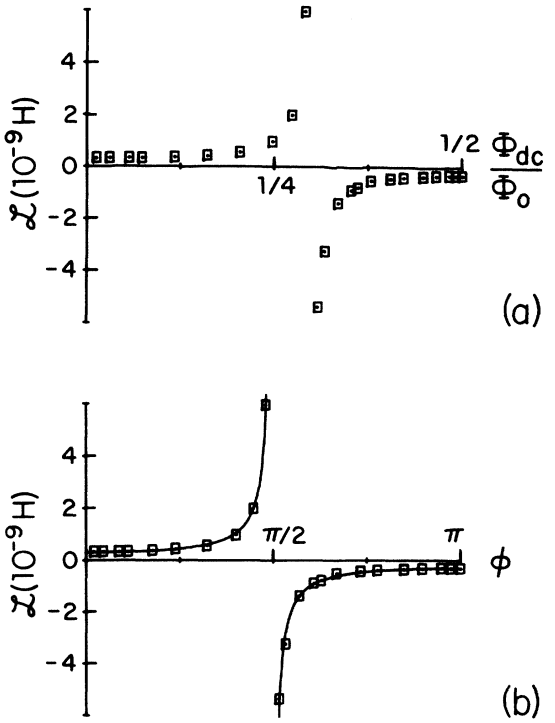


FIG. 6. (a) Plot of $\mathcal{L}$ vs $\Phi_{dc}/\Phi_0$ for point contact with $I_c \approx 1.1\,\mu$A. The horizontal axis has been shifted so that the origin corresponds to an integral number of $\Phi_0$ in the ring. (b) Plot of $\mathcal{L}(\phi)$ from above data using $\phi(\Phi_{dc})$ calculated from Eq. (15). Solid line is $\Phi_0/2\pi I_c \cos\phi$ with $I_c = 1.1\,\mu$A.

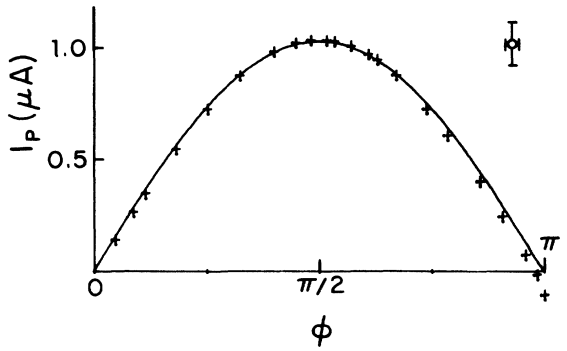


FIG. 7. Plot of $I_p(\phi)$ calculated from data of Fig. 6(a). Solid line is $I = I_c \sin\phi$ with $I_c = 1.1\ \mu$A. The bars on the point inset indicate the estimated uncertainties for each point.

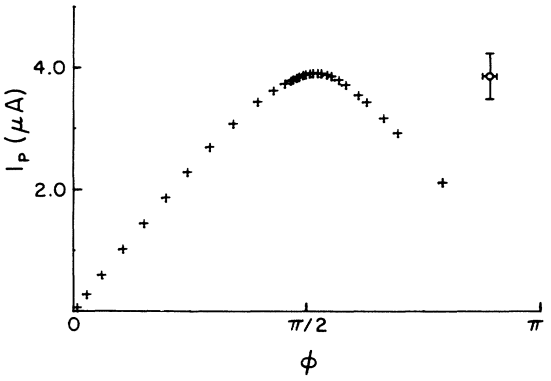


FIG. 9. Plot of $I_p(\phi)$ calculated from data of Fig. 8. The bars on the point inset indicate the estimaed uncertainties for each point.

is singular at $\Phi_{dc}$ only slightly greater than $\frac{1}{4}\Phi_0$ indicating that indeed there was only a small screening flux $LI$. The singularity is followed by the expected negative-inductance region.[12]

Figure 6(b) shows the same data but now expressed as $\mathcal{L}(\phi)$ by using the $\phi(\Phi_{dc})$ obtained from Eq. (14). Here the data are almost precisely antisymmetric about $\phi = \frac{1}{2}\pi$. The solid line plotted in the figure is the function $\Phi_0/2\pi I_c \cos\phi$ with $I_c = 1.1\ \mu$A; the good fit indicates that the current-phase relation is almost sinusoidal. For point contacts in this group the inductance can be measured over the entire range $0 \leq \phi \leq \pi$ because $\epsilon \equiv 2\pi I_c L/\Phi_0$ is less than unity and as a result $\phi(\Phi_{dc})$ is a continuous function. The current-phase relation shown in Fig. 7 (crosses) were calculated from the same data shown in Figs. 5 and 6 and indeed is nearly sinusoidal.

Data representative of the second group of point contacts are shown in Fig. 8. The effects of the large screening flux is apparent from the large displacement of the singularity to the right of $\frac{1}{4}\Phi_0$. In this case only the initial portion of the

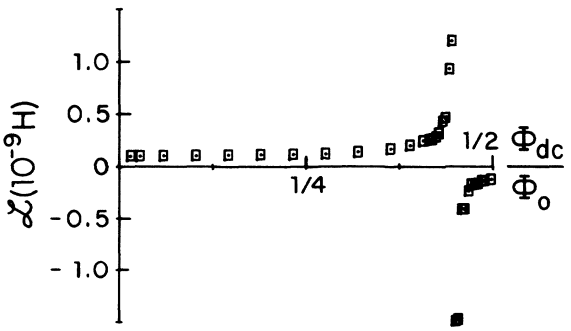


FIG. 8. Plot of $\mathcal{L}$ vs $\Phi_{dc}/\Phi_0$ for point contact with $I_c \approx 4\ \mu$A. The horizontal axis has been shifted so that the origin corresponds to an integral number of $\Phi_0$ in the ring.

negative inductance curve is obtained reliably since with the large screening flux the function $\phi(\Phi_{dc})$ becomes discontinuous. This discontinuity is not immediately obvious in the $\mathcal{L}(\Phi_{dc})$ data which are quite smooth, but becomes apparent on evaluating $\phi(\Phi_{dc})$ from Eq. (14) since $\phi$ does not reach $\pi$ when $\Phi_{dc}$ is integrated up to $\frac{1}{2}\Phi_0$. The current-phase relation calculated from the data of Fig. 8 is shown in Fig. 9 and it is correspondingly truncated. This curve is a measure of current-phase relation only up to some value $\Phi_{dc} = (\Phi_{dc})_J$ at which the discontinuity in $\phi(\Phi_{dc})$ occurred.

The precise value of $(\Phi_{dc})_J$ cannot be obtained without *a priori* knowledge of the current-phase relation. However an estimate can be obtained by assuming $I_p(\phi) = I_c \sin\phi$, using Eq. (3) to calculate $\phi(\Phi_{dc})$, and finding the value $(\Phi_{dc})_J$ at which $\phi(\Phi_{dc})$ becomes multivalued and at which a jump in $\phi$ would lead to a lower energy $E = -(\Phi_0 I_c/2\pi)\cos\phi + \frac{1}{2}LI^2$ for the ring. With $I_c = 4.1\ \mu$A and $L = 1.0 \times 10^{-10}$ H we estimate $(\Phi_{dc})_J = 0.48\Phi_0$ corresponding to $\phi = 1.9$. Thus for the data of Fig. 8 we expect that for $0 < \Phi_{dc} < 0.48\Phi_0$ the measured $\mathcal{L}$ corresponds to the continuous variation of $\phi$ from 0 to 1.9. However for $\Phi_{dc} > 0.48\Phi_0$ the measured $\mathcal{L}$ corresponds to the variation of $\phi$ some where in the range $\pi < \phi < \frac{3}{2}\pi$.

The jump in phase would in general produce a discontinuity in $\mathcal{L}(\Phi_{dc})$; however, fluctuations in $\phi$ are expected to produce some averaging that leads to a continuous variation for the actual measured values of $\mathcal{L}$. In addition the rf measuring current produces an additional small dither in $\Phi_{dc}$, so the measured $\mathcal{L}$ corresponds to some average of the values of $\mathcal{L}$ appropriate to the second and third quadrants of $I(\phi)$. As a result of this discontinuous variation of $\phi$, the values of $\phi(\Phi_{dc})$ and consequently of $I(\phi)$ in Fig. 9 are not expected to be valid beyond $\phi \simeq 1.9$. Calculations

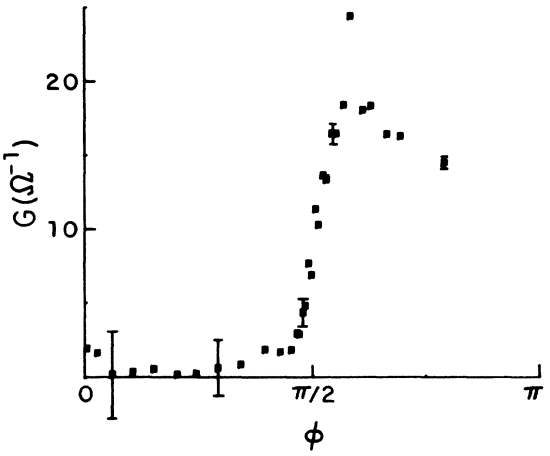


FIG. 10. Plot of $G(\phi)$ for point contact for which $\mathcal{L}(\Phi_{dc})$ is shown in Fig. 8. Estimated uncertainties are shown by the bars on five representative points.

using an assumed sinusoidal current-phase relation to estimate the expected variation of $\mathcal{L}$ after the jump give qualitatively the observed variation of $\mathcal{L}(\Phi_{dc})$ and a reasonable explanation for the shape and incompleteness of the $I(\phi)$ curve calculated from the $\mathcal{L}(\Phi_{dc})$ data.

Our discussion of the discontinuous behavior of $\phi(\Phi_{dc})$ is an oversimplification of a problem that has been analyzed in detail by Kurkijarvi,[13] Kurkijarvi and Webb,[14] and Jackel, Buhrman, and Webb.[4] However the discussion probably suffices to establish an estimate of $(\Phi_{dc})_J$ that is adequate for interpreting the data.

For point-contacts in this second group the conductance $G$ was large enough to be measured. Experimental values for $G(\phi)$ are shown in Fig. 10 for the same point contact for which the $\mathcal{L}(\Phi_{dc})$ data are shown in Fig. 8. By inserting values for the various circuit parameters into Eq. (11) it can be seen that for small values of $\phi$ the measured quantity $R_{eff}$ is not very sensitive to $G$; however, the sensitivity increases as $\phi$ approaches $\frac{1}{2}\pi$. Correspondingly small uncertainties in the measured values of $R_{eff} - R_T$ result in very large uncertainties in the experimentally determined $G(\phi)$ as indicated by the error bars in Fig. 10. Thus, although the conductance $G$ is probably nonzero for small $\phi$ we cannot distinguish it from zero within the accuracy of the measurements in that range of $\phi$. However, the data do indicate a phase-dependent conductance that is an increasing function of $\phi$ up to $\phi = 1.9$. Although the data in Fig. 10 are not well represented by the function $G(\phi) = G_0(1 + \alpha\cos\phi)$, to achieve even qualitative agreement so that $G$ increases for $0 < \phi < 1.9$ requires a negative value for $\alpha$. The data are also consistent with the form of $G(\phi)$ obtained from a simple phenomenological model[15] which predicts it to be an increasing function of $0 < \phi < \pi$.

As discussed above, for this data for $\phi > 1.9$ it is very likely that there was a jump in $\phi$ so that the data plotted for $1.9 < \phi < \pi$ actually correspond to $\pi < \phi < \frac{3}{2}\pi$. The decrease in the experimental values of $G$ in Fig. 10 for $\phi > 1.9$ are consistent with this interpretation since the function $G(\phi)$ would be predicted to decrease in the range $\pi < \phi < \frac{3}{2}\pi$ either with negative $\alpha$ or using the phenomenological model.

The general behavior of the data for all point contacts in this second group was like that shown in Fig. 10 and the data require a phase-dependent conductance. However, the accuracy of the data is not sufficient to determine a particular function $G(\phi)$. In part the inaccuracy may arise from the inadequacies of our idealized circuit model which can lead to errors in determining $R_{eff} - R_T$ when $R_{eff} \simeq R_T$.

For point contacts with critical currents greater than 5 $\mu$A we find that the measured $I_p(\phi)$ curve (analogous to Fig. 9) peaks well before $\frac{1}{2}\pi$. For this range of $I_c$, $\phi(\Phi_{dc})$ is discontinuous near $\frac{1}{2}\pi$, and the effect of averaging the impedance $\mathcal{L}(\phi)$ over the hysteretic portion is more pronounced than it was for the smaller $I_c$. The data do not mean that the actual current-phase relation is necessarily nonsinusoidal, but fluctuations can result in an averaged impedance which in turn can yield an apparent $I_p(\phi)$ that is very nonsinusoidal.

## IV. CONCLUSIONS

The experiments described above demonstrate that both the current-phase relation and the phase-dependent conductance can be obtained simultaneously using ac techniques. The measurements show the validity of representing the weak link as a phase-dependent impedance in the small-signal limit. The use of phase bias permitted a continuous mapping of the impedance for $0 \leq \phi \leq 2\pi$ thereby enabling us to observe the entire negative-inductance branch.

For point contacts with sufficiently small critical currents we found good agreement with a sinusoidal current-phase relation. For point contacts with larger critical currents we were able to resolve a phase-dependent conductance with sufficient accuracy to determine that it was an increasing function of phase at least for $0 < \phi < 1.9$ and hence was consistent with a negative coefficient for the $\cos\phi$ term. For large critical currents the measured current-phase relation, particularly in the discontinuous mode, was consistent with that expected to be produced by fluctuations. Experiments of this type may be another useful technique for studying the effects of fluctuations.

ACKNOWLEDGMENTS

We would like to thank Ashley Vincent for his assistance with the initial experiments and Li-Kong Wang and Vittorio Celli for their assistance with some of the calculations. We also appreciate several helpful discussions with L. D. Jackel.

---

*Research supported by the National Science Foundation.

[1]B. D. Josephson, Rev. Mod. Phys. 36, 216 (1964); Adv. Phys. 14, 419 (1965).

[2]T. A. Fulton and R. C. Dynes, Phys. Rev. Lett. 25, 794 (1970).

[3]J. R. Waldram and J. M. Lumley, Rev. Phys. Appl. 10, 7 (1975).

[4]L. D. Jackel, R. A. Buhrman, and W. W. Webb, Phys. Rev. B 10, 2782 (1974).

[5]N. F. Pedersen, T. F. Finnegan, and D. N. Langenberg, Phys. Rev. B 6, 4151 (1972).

[6]C. M. Falco, W. H. Parker, and S. E. Trullinger, Phys. Rev. Lett. 31, 933 (1973).

[7]D. A. Vincent and B. S. Deaver, Jr., Phys. Rev. Lett. 32, 212 (1974).

[8]M. Nisenoff and S. Wolf, Phys. Rev. B 12, 1712 (1975).

[9]D. N. Langenberg, Rev. Phys. Appl. 9, 35 (1974).

[10]R. E. Harris, Phys. Rev. B 10, 84 (1974).

[11]A. H. Silver and J. E. Zimmerman, Phys. Rev. 157, 317 (1967).

[12]P. V. Christiansen, E. B. Hansen, and C. J. Sjöström, J. Low Temp. Phys. 4, 349 (1971).

[13]J. Kurkijarvi, Phys. Rev. B 6, 832 (1972).

[14]J. Kurkijarvi and W. Webb, in *Proceedings of the 1972 Applied Superconductivity Conference* IEEE Pub. No. 72 CHO 682-5-TABSC (IEEE, New York, 1972), p. 581.

[15]B. S. Deaver, Jr., R. D. Sandell, and D. A. Vincent, Phys. Lett. A 46, 411 (1974).